Nonlinear Dyn (2018) 91:2331–2345
https://doi.org/10.1007/s11071-017-4016-x

ORIGINAL PAPER

Integrated distributed formation flight control with aerodynamic constraints on attitude and control surfaces

Xueyuan Wang · Hao Fang · Lihua Dou · Bin Xin · Jie Chen

Received: 8 June 2017 / Accepted: 15 December 2017 / Published online: 15 January 2018

Abstract This paper investigates a 3-D leader-following formation control problem for a group of missiles with aerodynamic constraints. To cope with the large maneuvering formation flight in bank-to-turn control mode, an integrated backstepping-based distributed control scheme, combining the inner-loop attitude manipulation and outer-loop formation control, is proposed. Command filters are introduced to handle the control surface saturations caused by the physical limitations, and the attitude constraints derived from the coordinated turn requirements. In addition, the B-spline neural networks are adopted to reconstruct the uncertain aerodynamic force and moment coefficients, of which the unknown parameters are then online learned by the adaptive tuning laws. The proposed integrated distributed formation control protocol will guarantee that all states in the closed-loop systems are cooperatively semi-globally uniformly ultimately bounded. The formation tracking errors can converge into a small region around zero by properly adjusting the control parameters. Finally, numerical simulations are conducted to demonstrate the effectiveness of the proposed control scheme.

X. Wang · H. Fang (✉) · L. Dou · B. Xin · J. Chen
Key Laboratory of Intelligent Control and Decision of Complex Systems, School of Automation, Beijing Institute of Technology, Beijing 100081, China
e-mail: fangh@bit.edu.cn

Keywords 3-D formation control · Distributed control · Backstepping · Command filter · B-spline neural network

1 Introduction

The past two decades have witnessed the rapid development of the advanced anti-missile systems, such as the surface-to-air missile systems and close-in weapon systems (CIWS). With the traditional single missile attack mode, missiles are faced with great challenges to survive from the hostile interceptions and electronic countermeasures. Under these circumstances, the multi-missile cooperative engagement is a good option to improve the penetration capability. A missile formation with a reasonable structure and efficient communication will be rather deceptive to the defense systems, which makes it difficult to distinguish and intercept. Hence, it is of great theoretical and practical significance to investigate the missile formation control problem.

Due to the promising prospect in the modern warfare, the multi-missile cooperative engagement problem has been studied extensively in past decades. Most of the literatures focused on the cooperative guidance problem [1–5] whose objective is to coordinate the impact time so that a group of missiles can simultaneously intercept the target at a desirable time. Meanwhile, generating and maintaining an appropriate formation in midcourse flight is also necessary for pene-

tration and other tactical purposes in the multi-missile cooperative engagement. Several attempts have been made to deal with the missile formation control problem. Cui et al. [6] proposed a three-loop missile formation control scheme, in which the formation controllers were designed using the dynamic inversion approach. In [7], the flight path angles and the differences between the leader's and the followers' heading angles were regarded as small quantities; meanwhile, the leader's states were treated as perturbations. The formation keeping controllers were then derived based on the small disturbance linearization and PI optimal control theory. Furthermore, Wei et al. [8] extended the results in [7] to deal with the formation keeping problem on condition that the leader's information was unavailable. According to the adaptive control model by separating the leader's motion states from the relative motion model, the unknown parameters of the leader were estimated by an adaptive adjustment regulation, which was further applied to the formation keeping controller. In addition, other approaches including the nonlinear model predictive control [9,10], L_1 adaptive control [11] and constraint force method [12] were also adopted in the formation flight control problem.

The existing formation flight control methods often adopt a two-loop control scheme including the outer-loop formation control and the inner-loop attitude control. Under the assumption that the attitude controllers are well designed to follow the commands generated from the formation controllers, the inner- and outer-loop control laws can be designed separately neglecting the interactions between them. This assumption is satisfied if the autopilot time constants are small enough, which presents a high demand on the response speed of the autopilots. However, this requirement can hardly be met when the missiles are in large maneuvering flight which is unavoidable in the formation flight control. Moreover, designing the inner- and outer-loop controllers separately is actually based on the timescale separation of dynamics and kinematics, which will introduce modeling errors as the systems are originally coupled [13]. So the formation control and the attitude control should be integrated to guarantee the closed-loop stability for all the flight conditions. Nevertheless, following this way, the model includes both kinematics and dynamics of the missile, which results in a high-order nonlinear system. This poses new challenges to the controller design.

Since the missiles considered in this paper are controlled using the bank-to-turn (BTT) technique, the attitude angles and control surfaces of the missiles are constrained due to the coordinated bank-to-turn requirements and some physical limitations. This is another motivation to integrate the two control loops. Because the aerodynamic constraints imposed on the missile dynamics cannot be fully covered in the design of the formation control law if the two control loops are designed separately. The cooperative control problem, subject to the state and actuator constraints, has been extensively investigated. Some of them [14–16] only considered the actuator constraints, while others focused on handling the state constraints [17]. The nonlinear model predictive control (NMPC) [18] technique is commonly employed to deal with both state and actuator constraints for the cooperative control of nonlinear systems in the existing literatures. However, it may not satisfy the real-time requirement of the formation flight control system because the optimization process in NMPC would be time-consuming for the high-order aerodynamic system. Therefore, a proper method which is suitable to tackle with the state and actuator constraints in the cooperative control of the high-order nonlinear systems should be proposed.

In this paper, a leader-following formation flight control problem under a fixed directed graph is considered for multiple BTT missiles subject to the constraints on attitude angles and control surface deflections. Due to the complex flight conditions (e.g., electronic jamming and spoofing) and the limited communication capability of the omnidirectional antenna, it is rather difficult to guarantee that all the followers can obtain information directly from the leader. Thus, a distributed scheme is applied to the leader-following structure in this study. To be more specific, very few followers can utilize the information of the leader in the control law, while others can only use the information of the neighboring followers. In addition, the command filters [19–21] are adopted in this paper so that the state and actuator constraints will not be violated and the real-time requirement of the formation control problem is also satisfied.

The main contributions of this work are as follows.

– Unlike the two-loop or three-loop control scheme in the existing works [6,7,12] on formation flight, we proposed an integrated formation control scheme, which can address the formation control and atti-

tude control problems simultaneously, and guarantee the closed-loop stability of the whole flight control system theoretically.
- The proposed formation control algorithm is distributed, which is suitable for missiles due to the limited communication range. And each follower does not need to know the whole configuration of the formation, instead they only need to keep the relative positions from their neighbors, which makes the algorithm flexible and scalable.
- The proposed formation control protocol is able to deal with the uncertain aerodynamic coefficients in the missile dynamic systems and the aerodynamic constraints on the attitude and control surfaces which stem from the BTT control mode and some physical limitations.

The rest of this paper is organized as follows. Some preliminaries and problem formulations are stated in Sect. 2. A novel integrated distributed formation control scheme is proposed in Sect. 3, and the closed-loop stability is analyzed in Sect. 4. In Sect. 5, two numerical simulations are presented to verify the effectiveness of the proposed control approach. Finally, the conclusions are given in the last section.

2 Preliminaries and problem formulation

In this section, some necessary notions from the algebraic graph theory are briefly introduced at first. Then the reference frames, kinematic and dynamic models of the missiles, and B-spline neural networks, which are employed to reconstruct the uncertain aerodynamic coefficients, are then introduced. The formulation of the formation control problem is given at the end of this section.

2.1 Algebraic graph theory

In this paper, the communication topology for N followers is represented as a directed graph $\mathcal{G} = \{\mathcal{V}, \mathcal{E}\}$, where $\mathcal{V} = \{1, 2, \ldots, N\}$ is the node set and $\mathcal{E} \subseteq \mathcal{V} \times \mathcal{V}$ is the edge set. The directed edge (i, j) in $\mathcal{E}$ denotes that node j can obtain information from node i. $\mathcal{N}_i = \{j \in \mathcal{V} : (j, i) \in \mathcal{E}, j \neq i\}$ is the set of neighbors of node i. The adjacency matrix $\mathcal{A} = [a_{ij}] \in \mathbb{R}^{N\times N}$ of $\mathcal{G}$ is defined such that $a_{ij} = 1$ if $(j, i) \in \mathcal{E}$ and $a_{ij} = 0$ if $(j, i) \notin \mathcal{E}$. $\mathcal{L} \triangleq \mathcal{D} - \mathcal{A} \in \mathbb{R}^{N\times N}$ is the Laplacian matrix associated with $\mathcal{G}$, where $\mathcal{D} = [d_{ij}] \in \mathbb{R}^{N\times N}$ is the in-degree matrix given as $d_{ij} = 0, i \neq j$ and $d_{ii} = \sum_{j=1}^{N} a_{ij}, i = 1, \ldots, N$. The communication topology between the N followers and the leader is represented as an extended directed graph $\bar{\mathcal{G}} = \{\bar{\mathcal{V}}, \bar{\mathcal{E}}\}$, where $\bar{\mathcal{V}} = \{0, 1, 2, \ldots, N\}$ (node 0 stands for the leader) and $\bar{\mathcal{E}} \subseteq \bar{\mathcal{V}} \times \bar{\mathcal{V}}$. The Laplacian matrix $\bar{\mathcal{L}}$ associated with $\bar{\mathcal{G}}$ is defined as

$$\bar{\mathcal{L}} = \begin{bmatrix} 0 & 0_{1\times N} \\ -b & \mathcal{L} + \mathcal{B} \end{bmatrix} \tag{1}$$

where $b = [b_1, \ldots, b_N]^{\mathrm{T}}$, $\mathcal{B} = \mathrm{diag}\{b_1, \ldots, b_N\}$, $b_i = 1$ if $0 \in \mathcal{N}_i$ and $b_i = 0$ if $0 \notin \mathcal{N}_i, i = 1, 2, \ldots, N$. If there is at least one node named root node which has a directed path to all the other nodes, then the directed graph includes a directed spanning tree. If a directed graph has a directed spanning tree, the Laplacian matrix has the following property.

Lemma 1 ([22]) *The Laplacian matrix of a directed graph has a simple zero eigenvalue and all of the other eigenvalues are in the open right half plane if and only if the directed graph has a directed spanning tree.*

2.2 Model description

The models of the N followers are described with the aid of four reference frames in this paper: the earth-fixed reference frame $F_E(A - X_E Y_E Z_E)$, which is an inertial frame with its x-axis pointing to the north, z-axis pointing to the east; the trajectory-axis reference frame $F_T(O - X_T Y_T Z_T)$, transformed from F_E by two rotations of heading angle ψ_{V_i} and flight path angle θ_i; the velocity-axis reference frame $F_V(O - X_V Y_V Z_V)$, obtained from F_T by a rotation of bank angle γ_{V_i}; the body-axis reference frame $F_B(O - X_B Y_B Z_B)$, transformed from F_V by two successive rotations of sideslip angle β_i and angle of attack α_i. The reference frames mentioned above are all depicted in Fig. 1. More details about the reference frames and transformation matrices can be found in [23].

In what follows, it is assumed that the missile is a single rigid body, neglecting the effects of structural deflections (aeroelasticity) and the relative motion of the control surfaces. The air is assumed to be at rest, neglecting any effect caused by wind. It is also assumed that the earth is flat and the mass of the missile is constant. In addition, the flight path angle θ_i is assumed to satisfy $|\theta_i| < \theta_m (\theta_m < \frac{\pi}{2})$ during the flight. Under

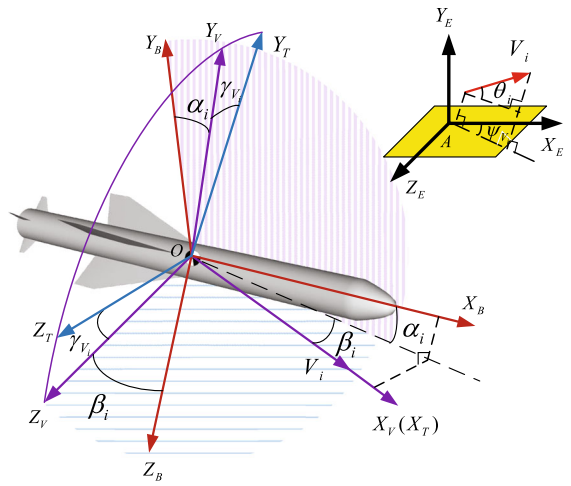

Fig. 1 Missile reference frames

these assumptions, the 6-DOF nonlinear aerodynamic models of the ith follower are given as follows [23].

First, the kinematic models of the follower i are

$$\dot{X}_{i,1} = G_{i,1}(X_{i,2}) \tag{2}$$

$$\dot{X}_{i,2} = H_{i,1} + G_{i,2}\left(X_{i,3}, P_i\right) \tag{3}$$

where

$$G_{i,1}(X_{i,2}) = \begin{bmatrix} V_i \cos\theta_i \cos\psi_{V_i} \\ V_i \sin\theta_i \\ -V_i \cos\theta_i \sin\psi_{V_i} \end{bmatrix},$$

$$H_{i,1} = \begin{bmatrix} -g\sin\theta_i \\ -g\cos\theta_i / V_i \\ 0 \end{bmatrix},$$

$$G_{i,2}(X_{i,3}, P_i) = \begin{bmatrix} \frac{P_i \cos\alpha_i \cos\beta_i - D_i}{m_i} \\ \frac{P_i(\sin\alpha_i \cos\gamma_{V_i} + \cos\alpha_i \sin\beta_i \sin\gamma_{V_i}) + L_i \cos\gamma_{V_i} - Y_i \sin\gamma_{V_i}}{m_i V_i} \\ -\frac{P_i(\sin\alpha_i \sin\gamma_{V_i} - \cos\alpha_i \sin\beta_i \cos\gamma_{V_i}) + L_i \sin\gamma_{V_i} + Y_i \cos\gamma_{V_i}}{m_i V_i \cos\theta_i} \end{bmatrix},$$

$X_{i,1} = [x_i, y_i, z_i]^{\mathrm{T}}$, $X_{i,2} = [V_i, \theta_i, \psi_{V_i}]^{\mathrm{T}}$, $i = 1, \ldots, N$. x_i, y_i and z_i are the coordinates of each missile in the earth-fixed inertial frame. V_i denotes the velocity. θ_i and ψ_{V_i} are used to determine the direction of V_i. P_i is the engine thrust. D_i, Y_i and L_i denote the drag, side force and lift, respectively, which can be expressed in the following form:

$$\begin{cases} D_i = q_i S_i C_{D_i} \\ Y_i = q_i S_i C_{Y_i} \\ L_i = q_i S_i C_{L_i} \end{cases} \tag{4}$$

where q_i is the dynamic pressure and S_i is the aerodynamic reference area of the missile. q_i can be calculated through $q_i = \frac{1}{2}\rho_i V_i^2$, where ρ_i is the average density of air. C_{D_i}, C_{Y_i} and C_{L_i} are the drag, lift and side force coefficients, respectively, which can be expressed in terms of the aerodynamic derivatives:

$$\begin{cases} C_{D_i} = C_{D_{i0}}(V_i) + C_{D_i}^{\alpha_i}(\alpha_i, V_i)\,|\alpha_i| \\ C_{Y_i} = C_{Y_i}^{\beta_i}(\alpha_i, V_i)\beta_i \\ C_{L_i} = C_{L_{i0}}(V_i) + C_{L_i}^{\alpha_i}(\alpha_i, V_i)\alpha_i \end{cases} \tag{5}$$

where $C_{D_{i0}} = C_{D_i}|_{\alpha_i=0}$ and $C_{L_{i,0}} = C_{L_i}|_{\alpha_i=0}$. $C_{D_i}^{\alpha_i}$ is defined as $C_{D_i}^{\alpha_i} = \partial C_{D_i}/\partial\alpha_i$, and other coefficients are defined similarly. These coefficients can be modeled as functions with respect to some of the flight conditions (i.e., α_i and V_i).

Then, the dynamic models of the follower i are

$$\dot{X}_{i,3} = A_{i,2}F_{i,1}(X_i) + H_{i,2} + B_{i,1}X_{i,4} \tag{6}$$

$$\dot{X}_{i,4} = A_{i,3}F_{i,2}(X_i) + H_{i,3} + B_{i,2}U_i \tag{7}$$

where

$$A_{i,2} = \frac{1}{m_i V_i}\begin{bmatrix} 0 & 0 & -1/\cos\beta_i \\ 0 & 1 & 0 \\ 0 & \tan\theta_i \cos\gamma_{V_i} & \tan\beta_i + \tan\theta_i \sin\gamma_{V_i} \end{bmatrix},$$

$$H_{i,2} = \frac{1}{m_i V_i}\begin{bmatrix} \left(m_i g\cos\theta_i \cos\gamma_{V_i} - P_i \sin\alpha_i\right)/\cos\beta_i \\ m_i g\cos\theta_i \sin\gamma_{V_i} - P_i\cos\alpha_i \sin\beta_i \\ -m_i g\tan\beta_i \cos\theta_i \cos\gamma_{V_i} + P_i r_i \end{bmatrix},$$

$$B_{i,1} = \begin{bmatrix} -\tan\beta_i\cos\alpha_i & \sin\alpha_i\tan\beta_i & 1 \\ \sin\alpha_i & \cos\alpha_i & 0 \\ \sec\beta_i\cos\alpha_i & -\sec\beta_i\sin\alpha_i & 0 \end{bmatrix},$$

$$H_{i,3} = \begin{bmatrix} (J_{yi} - J_{zi})\omega_{zi}\omega_{yi}/J_{xi} \\ (J_{zi} - J_{xi})\omega_{xi}\omega_{zi}/J_{yi} \\ (J_{xi} - J_{yi})\omega_{yi}\omega_{xi}/J_{zi} \end{bmatrix},$$

$$F_{i,2}(X_i) = [M_{xi0}, M_{yi0}, M_{zi0}]^{\mathrm{T}} = q_i S_i \begin{bmatrix} l_i\left[m_{xi}^{\beta_i}(\beta_i)\beta_i + m_{xi}^{\omega_{xi}}(V_i)\omega_{xi}\right] \\ l_i\left[m_{yi}^{\beta_i}(\beta_i)\beta_i + m_{yi}^{\omega_{yi}}(V_i)\omega_{yi}\right] \\ b_{Ai}\left[m_{zi}^{\alpha_i}(\alpha_i)\alpha_i + m_{zi}^{\omega_{zi}}(V_i)\omega_{zi}\right] \end{bmatrix},$$

$F_{i,1}(X_i) = [D_i, Y_i, L_i]^{\mathrm{T}}$, $A_{i,3} = \mathrm{diag}\{J_{xi}, J_{yi}, J_{zi}\}^{-1}$, $r_i = \tan\beta_i \sin\alpha_i - \tan\theta_i \cos\gamma_{V_i}\cos\alpha_i \sin\beta_i + \tan\theta_i \sin\alpha_i \sin\gamma_{V_i}$, $B_{i,2} = q_i S_i \mathrm{diag}\{m_{xi}^{\delta_{xi}} l_i/J_{xi}, m_{yi}^{\delta_{yi}} l_i/J_{yi}, m_{zi}^{\delta_{zi}} b_{Ai}/J_{zi}\}$, $X_{i,3} = [\alpha_i, \beta_i, \gamma_{V_i}]^{\mathrm{T}}$, $X_{i,4} = [\omega_{xi}, \omega_{yi}, \omega_{zi}]^{\mathrm{T}}$, and $X_i = [X_{i,1}^{\mathrm{T}}, X_{i,2}^{\mathrm{T}}, X_{i,3}^{\mathrm{T}}, X_{i,4}^{\mathrm{T}}]^{\mathrm{T}}$.

ω_{xi}, ω_{yi} and ω_{zi} are the roll, yaw and pitch rates with respect to the body-axis reference frame. $U_i =$

$[\delta_{xi}, \delta_{yi}, \delta_{zi}]^{\mathrm{T}}$ is the control surface deflection, where δ_{xi}, δ_{yi} and δ_{zi} represent the deflections of the aileron, rudder and elevator. l_i and b_{Ai} are the wing span and wing mean aerodynamic chord, respectively. J_{xi}, J_{yi} and J_{zi} are the roll, yaw and pitch moments of inertia. m^*_{xi}, m^*_{yi}, and m^*_{zi} are the rolling, yawing and pitching moment coefficients, in which $m^{\beta_i}_{xi}$ is defined as the partial derivative of the rolling moment coefficient m_{xi} with respect to β_i and other moment coefficients have similar definitions. The moment coefficients can also be regarded as the functions with respect to some of the flight conditions (i.e., α_i, β_i and V_i).

Assumption 1 The functions, representing the variation of the aerodynamic force and moment coefficients in Eqs. (5) and (7), are continuous in certain compact sets.

2.3 Approximation of the aerodynamic coefficients

The aerodynamic force and moment coefficients involved in the model are uncertain, so they need to be approximated before designing the formation controller. B-spline neural network (BSNN) is suitable for providing online aerodynamic coefficient approximation [24] due to the local support property [25] and the flexible choice on the order of the B-splines [26]. The aerodynamic coefficients will be transformed into linear-in-the-parameters form using B-spline functions as the basis vectors, and then, the parameters will be online learned by the adaptive update laws in this paper.

Since the aerodynamic coefficients which need to be approximated have similar characteristics, we take $C^{\alpha_i}_{D_i}(\alpha_i, V_i)$ in Eq. (5) as an example. Let $C^{\alpha_i}_{D_i}$ be continuous in a compact set $\Omega_{\mathcal{D}}$, then it can be approximated in the following form

$$\hat{C}^{\alpha_i}_{D_i}(\alpha_i, V_i) = \phi^{\mathrm{T}}_{D_{\alpha_i}}(\alpha_i, V_i)\hat{\theta}_{D_{\alpha_i}} \tag{8}$$

where $\hat{\theta}_{D_{\alpha_i}}$ denotes the estimate of the weight vectors which will be learned by the update laws and $\phi_{D_{\alpha_i}}(\alpha_i, V_i)$ is the B-spline basis vector defined as the tensor products of two univariate B-spline basis functions with respect to α_i and V_i, respectively. Defined on an interval with q equal subintervals, each univariate B-spline basis function consists of $(q+2)$ pieces of functions transformed from the Cardinal B-spline functions [26]. Other coefficients can be approximated in a similar form as Eq. (8).

The true function $C^{\alpha_i}_{D_i}(\alpha_i, V_i)$ can be written as

$$C^{\alpha_i}_{D_i}(\alpha_i, V_i) = \phi^{\mathrm{T}}_{D_{\alpha_i}}\theta^*_{D_{\alpha_i}} + \varepsilon_{D_{\alpha_i}} \tag{9}$$

where $\varepsilon_{D_{\alpha_i}}$ denotes the approximation error which can be made arbitrarily small by increasing the number of nodes in the BSNN. $\theta^*_{D_{\alpha_i}}$ denotes the optimal vector that minimizes the approximation error, which is defined as

$$\theta^*_{D_{\alpha_i}} = \arg\min_{\theta_{D\alpha_i}} \left\{ \sup_{\Omega_{\mathcal{D}}} \left| C^{\alpha_i}_{D_i}(\alpha_i, V_i) - \phi^{\mathrm{T}}_{D_{\alpha_i}}\theta_{D_{\alpha_i}} \right| \right\}. \tag{10}$$

Therefore, $F_{i,1}$, $F_{i,2}$ and $B_{i,2}$ are reconstructed as follows

$$\begin{aligned}\hat{F}_{i,1} &= \Phi^{\mathrm{T}}_{F_{i,1}}\hat{\Theta}_{F_{i,1}} \\ &= \mathrm{diag}\left\{\phi^{\mathrm{T}}_{D_i}, \phi^{\mathrm{T}}_{Y_i}, \phi^{\mathrm{T}}_{L_i}\right\}\left[\hat{\theta}^{\mathrm{T}}_{D_i}, \hat{\theta}^{\mathrm{T}}_{Y_i}, \hat{\theta}^{\mathrm{T}}_{L_i}\right]^{\mathrm{T}}\end{aligned} \tag{11}$$

$$\begin{aligned}\hat{F}_{i,2} &= \Phi^{\mathrm{T}}_{F_{i,2}}\hat{\Theta}_{F_{i,2}} \\ &= \mathrm{diag}\left\{\phi^{\mathrm{T}}_{M_{xi0}}, \phi^{\mathrm{T}}_{M_{yi0}}, \phi^{\mathrm{T}}_{M_{zi0}}\right\}\left[\hat{\theta}^{\mathrm{T}}_{M_{xi0}}, \hat{\theta}^{\mathrm{T}}_{M_{yi0}}, \hat{\theta}^{\mathrm{T}}_{M_{zi0}}\right]^{\mathrm{T}}\end{aligned} \tag{12}$$

$$\begin{aligned}\hat{B}_{i,2} &= \Phi^{\mathrm{T}}_{B_{i,2}}\hat{\Theta}_{B_{i,2}} \\ &= \mathrm{diag}\left\{\phi^{\mathrm{T}}_{M^{\delta_{xi}}_{xi}}, \phi^{\mathrm{T}}_{M^{\delta_{yi}}_{yi}}, \phi^{\mathrm{T}}_{M^{\delta_{zi}}_{zi}}\right\} \\ &\quad \mathrm{diag}\left\{\hat{\theta}_{M^{\delta_{xi}}_{xi}}, \hat{\theta}_{M^{\delta_{yi}}_{yi}}, \hat{\theta}_{M^{\delta_{zi}}_{zi}}\right\}\end{aligned} \tag{13}$$

where $\phi^{\mathrm{T}}_{D_i} = q_i S_i[\phi^{\mathrm{T}}_{D_{i0}}, \phi^{\mathrm{T}}_{D_{\alpha_i}}|\alpha_i|]$, $\hat{\theta}_{D_i} = [\hat{\theta}^{\mathrm{T}}_{D_{i0}}, \hat{\theta}^{\mathrm{T}}_{D_{\alpha_i}}]^{\mathrm{T}}$, and other ϕ_*s and $\hat{\theta}_*$s have similar definitions according to Eqs. (5) and (7). Moreover, the optimal weight vectors $\Theta^*_{F_{i,1}}$, $\Theta^*_{F_{i,2}}$ and $\Theta^*_{B_{i,2j}}$ exist such that the following inequalities hold.

$$\left\| F_{i,1} - \Phi^{\mathrm{T}}_{F_{i,1}}\Theta^*_{F_{i,1}} \right\| = \left\| E_{F_{i,1}} \right\| \leqslant e_{i,1} \tag{14}$$

$$\left\| F_{i,2} - \Phi^{\mathrm{T}}_{F_{i,2}}\Theta^*_{F_{i,2}} \right\| = \left\| E_{F_{i,2}} \right\| \leqslant e_{i,2} \tag{15}$$

$$\left\| B_{i,2j} - \Phi^{\mathrm{T}}_{B_{i,2j}}\Theta^*_{B_{i,2j}} \right\| = \left\| E_{B_{i,2j}} \right\| \leqslant e_{i,3j} \quad j = 1, 2, 3 \tag{16}$$

where $E_{F_{i,1}}$, $E_{F_{i,2}}$ and $E_{B_{i,2j}}$ are the reconstruction errors, which are bounded over the compact sets $\Omega_{F_{i,1}}$, $\Omega_{F_{i,2}}$ and $\Omega_{B_{i,2j}}$, respectively. The upper bounds $e_{i,1}$, $e_{i,2}$ and $e_{i,3j}$ are positive constants.

2.4 Problem formulation

Since the missile formation and attitude control are to be integrated to cope with the large maneuvering flight

condition, the kinematic models (2)–(3) and dynamic models (6)–(7) will be considered together as a fourth-order nonlinear system. Meanwhile, we notice that this nonlinear system is in a quasi strict-feedback form which inspires us to adopt the distributed backstepping scheme to address this problem. In this manner, the fourth-order nonlinear system will be treated as four nonlinear subsystems and the distributed formation control protocol is designed in a recursive way.

For a BTT missile, the most significant constraint is the allowable side-slip angle which should be kept in a small region around zero. Ideally, the side-slip angle should be zero, which would lead to completely coordinated turns. In addition, the angular rates and control surface deflections are constrained due to some physical limitations, and the other attitude angles are also limited to meet the requirements of BTT control mode, which will be discussed later in Sect. 3.

Let $y_i = X_{i,1}$ be the output of the ith follower. Then the formation tracking error e_f for the missile team composed of one leader and N followers can be defined as

$$e_f = y - y^d - (\mathbf{1}_N \otimes r) \tag{17}$$

where $y = [y_1^{\mathrm{T}}, \ldots, y_N^{\mathrm{T}}]^{\mathrm{T}}$, $y^d = [(y_{1r}^d)^{\mathrm{T}}, \ldots, (y_{Nr}^d)^{\mathrm{T}}]^{\mathrm{T}}$, $y_{ir}^d \in \mathbb{R}^3$ $(i = 1, \ldots, N)$ denotes the position of follower i relative to the leader in the predetermined formation, and $\mathbf{1}_N$ is a $N \times 1$ column vector of ones. If e_f can be controlled to be zero, the followers will maintain the predetermined formation and follow the trajectory of the leader precisely.

Therefore, the objective of this paper is to design a distributed formation control law (including the control surface deflection U_i and the thrust P_i) for each follower, such that the formation tracking error e_f converges into a small region around zero, while the attitude angles $X_{i,3}$, angular rates $X_{i,4}$ and control surfaces U_i are restricted in the compact sets $\Omega_{X_{i,3}}$, $\Omega_{X_{i,4}}$ and $\Omega_{U_i} \subset R^3$, respectively.

Assumption 2 The trajectory of the leader $r(t)$ and its first derivative $\dot{r}(t)$ are continuous and bounded. The extended graph $\bar{\mathcal{G}}$ contains a directed spanning tree.

3 Distributed formation controller design

In the integrated control scheme, the most challenging problem is that the leader-following formation flying and attitude control should be handled simultaneously. In other words, a high-order nonlinear cooperative control problem should be addressed. To solve this problem, an integrated distributed backstepping-based formation control method will be proposed in this section. In this integrated control method, the distributed formation virtual controller will be constructed to maintain a stable formation structure with respect to the first subsystem, and other subsystems are utilized to design controllers to guarantee that the commanded velocity, attitude angles and angular rates are accurately achieved. In each step, the virtual controllers will pass though the command filters to generate proper command states or control inputs, which satisfy the state constraints and actuator saturations, respectively. The additional compensating signals are used to compensate the errors resulting from the command filters and the disorder between the inner- and outer-loop control in large maneuvering flight.

Step 1: To derive a distributed formation controller, the communication topology information should be introduced into the formation tracking error, so that e_f will be decentralized in the following form

$$Z_1 = [(\mathcal{L} + \mathcal{B}) \otimes I_3][y - y^d - (\mathbf{1}_N \otimes r)] \tag{18}$$

where $Z_1 = [Z_{1,1}^{\mathrm{T}}, \ldots, Z_{N,1}^{\mathrm{T}}]^{\mathrm{T}}$ is the decentralized form of e_f for all the followers, I_3 denotes a three-dimensional identity matrix, and $\mathcal{B} = \mathrm{diag}\{b_1, \ldots, b_N\}$, in which $b_i = 1, i = 1, \ldots, N$, if the follower i can obtain information from the leader directly and $b_i = 0$, otherwise.

From Assumption 2, the communication topology $\bar{\mathcal{G}}$ contains a directed spanning tree, so the rank of $\bar{\mathcal{L}}$ is N according to Lemma 1. Since $\mathrm{Rank}([-b \quad \mathcal{L} + \mathcal{B}]) = N$ and the sum of all the column vectors of matrix $[-b \quad \mathcal{L} + \mathcal{B}]$ equals to $\mathbf{0}_N$, where $\mathbf{0}_N$ is a $N \times 1$ column vector of zeros, $\mathcal{L} + \mathcal{B}$ is invertible. Therefore, we can stabilize Z_1 instead of e_f because $e_f = [(\mathcal{L} + \mathcal{B}) \otimes I_3]^{-1} Z_1$.

According to Eq. (18), the formation tracking error corresponding to the ith follower can be expressed as

$$Z_{i,1} = \sum_{j \in \mathcal{N}_i} a_{ij} \left(y_i - y_j - y_{ij}^d \right) + b_i \left(y_i - r - y_{ir}^d \right) \tag{19}$$

where $y_{ij}^d \in \mathbb{R}^3$ denotes the position of follower i relative to the follower j in the predetermined formation, $r = [r_x, r_y, r_z]^{\mathrm{T}}$ represents the position of the leader and $\mathcal{N}_i$ stands for the neighbor set of follower i. a_{ij} is

the element of the adjacency matrix of graph $\mathcal{G}$. $a_{ij} = 1$ means follower i can receive information from follower j. If follower i cannot obtain information from follower j, $a_{ij} = 0$. With this term, $Z_{i,1}$ only contains the formation tracking errors with respect to the follower i's neighbors.

Taking the time derivative of $Z_{i,1}$, we obtain

$$\begin{aligned}\dot{Z}_{i,1} &= (b_i + d_{ii})G_{i,1}(X_{i,2}) \\ &\quad - \sum_{j\in\mathcal{N}_i} a_{ij}G_{j,1}(X_{j,2}) - b_i\dot{r}\end{aligned} \tag{20}$$

where $d_{ii} = \sum_{j=1}^{N} a_{ij}, i = 1, \ldots, N$.

To stabilize $Z_{i,1}$, the virtual controller $X_{i,2}^d$ for the ith follower is designed as

$$\begin{aligned}G_{i,1}(X_{i,2}^d) &= (g_{i,11}, g_{i,12}, g_{i,13})^{\mathrm{T}} \\ &= \frac{-K_{i,1}Z_{i,1} + \sum_{j\in\mathcal{N}_i} a_{ij}G_{j,1}(X_{j,2}) + b_i\dot{r}}{b_i + d_{ii}}\end{aligned} \tag{21}$$

where $K_{i,1}$ is a diagonal positive definite matrix. This virtual controller is distributed since it only uses the neighbors' information of follower i and the information of the leader if possible. With the condition that the flight path angle $\theta_i \in (-\pi/2, \pi/2)$ and the heading angle $\psi_{V_i} \in (-\pi, \pi]$, the components of $X_{i,2}^d = (V_i^d, \theta_i^d, \psi_{V_i}^d)^{\mathrm{T}}$ can be determined according to

$$V_i^d = \sqrt{g_{i,11}^2 + g_{i,12}^2 + g_{i,13}^2} \tag{22}$$

$$\psi_{V_i}^d = \begin{cases} -\arctan(g_{i,13}/g_{i,11}) & \text{if } g_{i,11} > 0 \\ -\pi - \arctan(g_{i,13}/g_{i,11}) & \text{if } g_{i,11} < 0,\ g_{i,13} > 0 \\ \pi - \arctan(g_{i,13}/g_{i,11}) & \text{if } g_{i,11} < 0,\ g_{i,13} < 0 \end{cases} \tag{23}$$

$$\theta_i^d = \arctan\frac{g_{i,12}}{\sqrt{g_{i,11}^2 + g_{i,13}^2}}. \tag{24}$$

For this high-order nonlinear system, the analytical expression of $\dot{X}_{i,2}^d$ contains complicated partial derivative terms, which will result in the explosion of complexity problem. To avoid this, the command filter technique is adopted to estimate $\dot{X}_{i,2}^d$. In this paper, the following second-order command filter [27] is used.

$$\ddot{x}^c = \omega_n^2\left[S_M(x^o) - x^c\right] - 2\zeta\omega_n\dot{x}^c \tag{25}$$

$$S_M(x) = \begin{cases} M_{\max} & x \geqslant M_{\max} \\ x & M_{\min} < x < M_{\max} \\ -M_{\min} & x \leqslant -M_{\min} \end{cases} \tag{26}$$

where x^o is the input of the command filter, $\dot{x}^c$ and x^c are the output, and ζ and ω_n represent the damping factor and the frequency, respectively. If the state $X_{i,2}$ is limited, it is reasonable that the desired state $X_{i,2}^d$ has the same limits. Thus, the magnitude limit function, denoted by $S_M(\cdot)$, is included in Eq. (25). The limits can be set to be infinity if no constraint is imposed on the state.

Note that if x^o is bounded, then x^c and $\dot{x}^c$ are bounded and continuous. In the linear range of the function $S_M(\cdot)$, the transfer function for the command filter from x^o to x^c is a second-order linear filter with unit dc gain defined as

$$\frac{X^c(s)}{X^o(s)} = \frac{\omega_n^2}{s^2 + 2\zeta\omega_n + \omega_n^2}. \tag{27}$$

Thus, when the limit functions are not in effect, the error $x^c - x^o$ can be made arbitrarily small by selecting ω_n to be sufficiently large. When the limit functions are in effect, the error $x^c - x^o$ is bounded because both x^c and x^o are bounded.

$X_{i,2}^c$ and $\dot{X}_{i,2}^c$, derived from passing $X_{i,2}^d$ through the command filter, are the command state of $X_{i,2}$ and its derivative, respectively. Then in order to eliminate the effect of the difference between $X_{i,2}^c$ and $X_{i,2}^d$ appeared when the limit functions in the command filter come into effect, the compensating signal $\xi_{i,1}$ is introduced as

$$\begin{aligned}\dot{\xi}_{i,1} &= -K_1\xi_{i,1} + (b_i + d_{ii})[G_{i,1}(X_{i,2}) \\ &\quad - G_{i,1}(X_{i,2}^d)].\end{aligned} \tag{28}$$

Thus, $Z_{i,1}$ is modified to $\bar{Z}_{i,1} = Z_{i,1} - \xi_{i,1}$, which is called the compensated formation tracking error. Differentiating $\bar{Z}_{i,1}$ and substituting Eqs. (21) and (28) into it, we get

$$\dot{\bar{Z}}_{i,1} = -K_{i,1}\bar{Z}_{i,1}. \tag{29}$$

Step 2: In this step, the virtual controller $X_{i,3}^d = (\alpha_i^d, \beta_i^d, \gamma_{V_i}^d)^{\mathrm{T}}$ and thrust P_i will be designed to eliminate the tracking errors of the velocity and its orientation angles for the ith follower defined by $Z_{i,2} = X_{i,2} - X_{i,2}^c$.

The time derivative of $Z_{i,2}$ is

$$\begin{aligned}\dot{Z}_{i,2} &= H_{i,1} + G_{i,2}(X_{i,3}, P_i) - \dot{X}_{i,2}^c \\ &= H_{i,1} + \hat{G}_{i,2}\left(X_{i,3}^d, P_i\right) \\ &\quad + \hat{G}_{i,2}(X_{i,3}, P_i) - \hat{G}_{i,2}\left(X_{i,3}^d, P_i\right) \\ &\quad + A_{i,1}\tilde{F}_{i,1} - \dot{X}_{i,2}^c\end{aligned} \tag{30}$$

where $A_{i,1}\tilde{F}_{i,1} = G_{i,2}(X_{i,3}, P_i) - \hat{G}_{i,2}(X_{i,3}, P_i)$,

$$A_{i,1} = \frac{1}{m_i V_i}\begin{bmatrix} -V_i & 0 & 0 \\ 0 & -\sin\gamma_{V_i} & \cos\gamma_{V_i} \\ 0 & -\dfrac{\cos\gamma_{V_i}}{\cos\theta_i} & -\dfrac{\sin\gamma_{V_i}}{\cos\theta_i} \end{bmatrix}, \tag{31}$$

$$\begin{aligned}\tilde{F}_{i,1} &= F_{i,1} - \hat{F}_{i,1} = \Phi_{F_{i,1}}^{\mathrm{T}}\Theta_{F_{i,1}}^{*} + E_{F_{i,1}} - \Phi_{F_{i,1}}^{\mathrm{T}}\hat{\Theta}_{F_{i,1}} \\ &= \Phi_{F_{i,1}}^{\mathrm{T}}\tilde{\Theta}_{F_{i,1}} + E_{F_{i,1}}.\end{aligned} \tag{32}$$

Select $\hat{G}_{i,2}(X_{i,3}^d, P_i) = (g_{i,21}, g_{i,22}, g_{i,23})^{\mathrm{T}}$ such that

$$\begin{aligned}\hat{G}_{i,2}\left(X_{i,3}^d, P_i\right) &= -H_{i,1} + \dot{X}_{i,2}^c - K_{i,2}Z_{i,2} - \frac{1}{2}\bar{Z}_{i,2} \\ &= \begin{bmatrix} \dfrac{P_i\cos\alpha_i^d\cos\beta_i^d - \hat{D}_i}{m_i} \\ \dfrac{P_i\left(\sin\alpha_i^d\cos\gamma_{V_i}^d + w_i\right) + \hat{L}_i\cos\gamma_{V_i}^d - \hat{Y}_i\sin\gamma_{V_i}^d}{m_i V_i} \\ -\dfrac{P_i\left(\sin\alpha_i^d\sin\gamma_{V_i}^d - w_i\right) + \hat{L}_i\sin\gamma_{V_i}^d + \hat{Y}_i\cos\gamma_{V_i}^d}{m_i V_i\cos\theta_i} \end{bmatrix}\end{aligned} \tag{33}$$

where $w_i = \cos\alpha_i^d\sin\beta_i^d\sin\gamma_{V_i}^d$, $K_{i,2}$ is a diagonal positive definite matrix, $\bar{Z}_{i,2} = Z_{i,2} - \xi_{i,2}$ is the compensated tracking error of $X_{i,2}$, and $\xi_{i,2}$ is the compensating signal which will be defined in Eq. (39).

Remark 1 In controller (33), the compensating signal $\xi_{i,2}$ actually serves as the feedback from the attitude control which will be discussed in the next step, so that the formation controller and attitude controller are integrated in this manner.

Since P_i and $X_{i,3}^d$ are not affine in $\hat{G}_{i,2}$, we will derive them according to Eq. (33). Note that, to achieve a coordinated turn for BTT missile, the desired sideslip angle β_i^d should be set to zero. Therefore, it is reasonable to set $\sin\beta_i^d = 0$ and $\hat{Y}_i = 0$ in Eq. (33). And since $\hat{D}_i$ and $\hat{L}_i$ can be decomposed as $\hat{D}_i = \hat{D}_{i0} + \hat{D}_{\alpha_i}|\alpha_i^d|$ and $\hat{L}_i = \hat{L}_{i0} + \hat{L}_{\alpha_i}\alpha_i^d$ according to Eqs. (4) and (5), we can get

$$\begin{cases} g_{i,21} = \dfrac{1}{m_i}\left(P_i\cos\alpha_i^d - \hat{D}_{i0} - \hat{D}_{\alpha_i}|\alpha_i^d|\right) \\ g_{i,22} = \dfrac{1}{m_i V_i}\left[\left(\hat{L}_{i0} + \hat{L}_{\alpha_i}\alpha_i^d + P_i\sin{\alpha_i}^d\right)\cos\gamma_{V_i}^d\right] \\ g_{i,23} = -\dfrac{1}{m_i V_i\cos\theta_i}\left[\left(\hat{L}_{i0} + \hat{L}_{\alpha_i}\alpha_i^d + P_i\sin{\alpha_i}^d\right)\sin\gamma_{V_i}^d\right]. \end{cases} \tag{34}$$

The missile we considered in this paper uses BTT 90 airframe, in which the lifting surface can be commanded to roll up to $\pm 90°$. Then $\gamma_{V_i}^d, {\alpha_i}^d$ and P_i will be derived through

$$\gamma_{V_i}^d = \begin{cases} -\pi/2 & \text{if } g_{i,x} = 0,\ g_{i,y} < 0 \\ \pi/2 & \text{if } g_{i,x} = 0,\ g_{i,y} > 0 \\ \arctan(g_{i,y}/g_{i,x}) & \text{otherwise.} \end{cases} \tag{35}$$

$$\tan\alpha_i^d\left[m_i g_{i,21} + \hat{D}\left(\alpha_i^d\right)\right] + \hat{L}(\alpha_i^d) = \frac{m_i g_{i,22} V_i}{\cos\gamma_{V_i}^d} \tag{36}$$

$$P_i = \frac{m_i g_{i,21} + \hat{D}\left(\alpha_i^d\right)}{\cos\alpha_i^d} \tag{37}$$

where $g_{i,x} = g_{i,22}m_i V_i$, $g_{i,y} = -g_{i,23}m_i V_i\cos\theta_i$, $\hat{D}(\alpha_i^d) = \hat{D}_{i0} + \hat{D}_{\alpha_i}|\alpha_i^d|$ and $\hat{L}(\alpha_i^d) = \hat{L}_{i0} + \hat{L}_{\alpha_i}\alpha_i^d$. Note that the intermediate control variable α_i^d can be obtained through numerically solving Eq. (36) according to the method in [28]. After obtaining α_i^d, P_i can be calculated by substituting α_i^d into Eq. (37).

Then substituting Eqs. (33) into (30), we have

$$\begin{aligned}\dot{Z}_{i,2} = &-K_{i,2}Z_{i,2} + A_{i,1}\tilde{F}_{i,1} + \hat{G}_{i,2}(X_{i,3}, P_i) \\ &- \hat{G}_{i,2}\left(X_{i,3}^d, P_i\right) - 0.5\bar{Z}_{i,2}.\end{aligned} \tag{38}$$

According to Eq. (6), if ω_{xi} is too large, α_i should be restricted to make $\dot{\beta}_i$ relatively small which enables the real value of β_i to stay in a small region around zero so that the roll and pitch channels are decoupled. $X_{i,3}^c$ and $\dot{X}_{i,3}^c$ can be derived by passing $X_{i,3}^d$ though the command filter in which $X_{i,3}^d$ is modified to meet the aforementioned constraints on $X_{i,3}$. The corresponding compensating signal $\xi_{i,2}$ is defined as

$$\dot{\xi}_{i,2} = -K_{i,2}\xi_{i,2} + \hat{G}_{i,2}(X_{i,3}, P_i) - \hat{G}_{i,2}\left(X_{i,3}^d, P_i\right). \tag{39}$$

Thus, using Eqs. (30) and (39), the derivative of $\bar{Z}_{i,2}$ is given by

$$\dot{\bar{Z}}_{i,2} = -(K_{i,2} + 0.5I_3)\bar{Z}_{i,2} + A_{i,1}\tilde{F}_{i,1}. \tag{40}$$

Step 3: In order to achieve the desired attitude $X_{i,3}^c$, the required angular rates $X_{i,4}^d = (\omega_{xi}^d, \omega_{yi}^d, \omega_{zi}^d)^{\mathrm{T}}$ will be designed in this step. The tracking error of the attitude is defined as $Z_{i,3} = X_{i,3} - X_{i,3}^c$. Using Eq. (6), the time derivative of $Z_{i,3}$ is

$$\dot{Z}_{i,3} = A_{i,2}F_{i,1} + H_{i,2} + B_{i,1}X_{i,4} - \dot{X}_{i,3}^c. \tag{41}$$

To stabilize $Z_{i,3}$, the virtual controller $X_{i,4}^d$ is designed as follows

$$X_{i,4}^d = B_{i,1}^{-1}\left(-A_{i,2}\hat{F}_{i,1} - H_{i,2} - K_{i,3}Z_{i,3} + \dot{X}_{i,3}^c - \frac{1}{2}\bar{Z}_{i,3}\right) \tag{42}$$

where $K_{i,3}$ is a diagonal positive definite matrix, $\bar{Z}_{i,3} = Z_{i,3} - \xi_{i,3}$, and $B_{i,1}$ is nonsingular because $|B_{i,1}| = -\sec\beta_i$ and β_i is guaranteed to stay in a small region around zero in step 2.

Now we will derive $X_{i,4}^c$ and $\dot{X}_{i,4}^c$ by passing $X_{i,4}^d$ though the command filter defined in Eq. (25), in which $X_{i,4}^d$ is modified to satisfy the limits of the angular rates. Then the third compensator of the command filter is defined as

$$\dot{\xi}_{i,3} = -K_{i,3}\xi_{i,3} + B_{i,1}\xi_{i,4} + B_{i,1}\left(X_{i,4}^c - X_{i,4}^d\right). \tag{43}$$

Taking derivative of $\bar{Z}_{i,3}$ and substituting Eqs.(41), (42) and (43) into it, we have

$$\dot{\bar{Z}}_{i,3} = -(K_{i,3} + 0.5I_3)\bar{Z}_{i,3} + A_{i,2}\tilde{F}_{i,1} + B_{i,1}\bar{Z}_{i,4}. \tag{44}$$

Step 4: In the final step, the desired angular rate $X_{i,4}^c$ will be achieved by directly manipulating the control surfaces of the missile (i.e., δ_{xi}, δ_{yi} and δ_{zi}). Taking time derivative of the angular rate tracking error $Z_{i,4} = X_{i,4} - X_{i,4}^c$ gives

$$\dot{Z}_{i,4} = A_{i,3}F_{i,2} + H_{i,3} + B_{i,2}U_i - \dot{X}_{i,4}^c. \tag{45}$$

Since $\hat{B}_{i,2}$ is nonsingular, the control law can be constructed as

$$U_i^d = \hat{B}_{i,2}^{-1}\left(-K_{i,4}Z_{i,4} - A_{i,3}\hat{F}_{i,2} - H_{i,3} + \dot{X}_{i,4}^c - B_{i,1}^{\mathrm{T}}\bar{Z}_{i,3} - 2\bar{Z}_{i,4}\right) \tag{46}$$

where $K_{i,4}$ is a diagonal positive definite matrix and $\bar{Z}_{i,4} = Z_{i,4} - \xi_{i,4}$ is the compensated tracking error of angular rate.

The desired control law (46) may not be applicable for the actuators due to the physical limitations on the servo motors. Hence, the executable control surface deflection U_i will be obtained by passing U_i^d through the fourth command filter. And the corresponding compensating signal $\xi_{i,4}$ is defined as

$$\dot{\xi}_{i,4} = -K_{i,4}\xi_{i,4} + \hat{B}_{i,2}\left(U_i - U_i^d\right). \tag{47}$$

With Eqs. (45)–(47), $\dot{\bar{Z}}_{i,4}$ is given by

$$\dot{\bar{Z}}_{i,4} = -(K_{i,4} + 2I_3)\bar{Z}_{i,4} + A_{i,3}\tilde{F}_{i,2} + \tilde{B}_{i,2}U_i - B_{i,1}^{\mathrm{T}}\bar{Z}_{i,3} \tag{48}$$

Remark 2 The controllers (33), (42) and (46), which are dedicated to track the command velocity, attitude angles and angular rates, only depend on the follower i's own states. So all the control laws designed in this section are distributed.

4 Stability analysis

Based on the analysis above, we will give the following theorem which indicates that the proposed integrated formation controllers can guarantee the closed-loop stability of the whole formation flight control system theoretically.

Theorem 1 *Under Assumptions 1 and 2, consider a team of agents including a leader and N followers described by (2), (3), (6) and (7). With the distributed control laws (21), (33), (42) and (46), command filters (25) and adaptive tuning laws*

$$\dot{\hat{\Theta}}_{F_{i,1}} = \Gamma_{F_{i,1}}\left[\Phi_{F_{i,1}}\left(A_{i,1}^{\mathrm{T}}\bar{Z}_{i,2} + A_{i,2}^{\mathrm{T}}\bar{Z}_{i,3}\right) - \mu_{F_{i,1}}\hat{\Theta}_{F_{i,1}}\right] \tag{49}$$

$$\dot{\hat{\Theta}}_{F_{i,2}} = \Gamma_{F_{i,2}}\left(\Phi_{F_{i,2}}A_{i,3}^{\mathrm{T}}\bar{Z}_{i,4} - \mu_{F_{i,2}}\hat{\Theta}_{F_{i,2}}\right) \tag{50}$$

$$\dot{\hat{\Theta}}_{B_{i,2j}} = \Gamma_{B_{i,2j}}\left(\Phi_{B_{i,2j}}\bar{Z}_{i,4}u_{i,j} - \mu_{B_{i,2j}}\hat{\Theta}_{B_{i,2j}}\right) \tag{51}$$

where $\mu_{F_{i,1}}, \mu_{F_{i,2}}, \mu_{B_{i,2j}} (i = 1, \ldots, N, j = 1, 2, 3)$ are small positive constants, the weight parameter errors $\tilde{\Theta}_{F_{i,1}}, \tilde{\Theta}_{F_{i,2}}, \tilde{\Theta}_{B_{i,2j}}$ and the tracking errors $Z_{i,l} (l = 1, \ldots, 4)$ for the ith follower are cooperatively semi-globally uniformly ultimately bounded (CSUUB). Furthermore, the formation tracking errors of all the followers will converge into a small neighborhood around zero by a proper choice of the control parameters.

Proof The Lyapunov function for the ith follower is chosen as

$$V_i = \frac{1}{2}\left(\sum_{k=1}^{4}\bar{Z}_{i,k}^{\mathrm{T}}\bar{Z}_{i,k} + \sum_{j=1}^{3}\tilde{\Theta}_{B_{i,2j}}^{\mathrm{T}}\Gamma_{B_{i,2j}}^{-1}\tilde{\Theta}_{B_{i,2j}} + \sum_{l=1}^{2}\tilde{\Theta}_{F_{i,l}}^{\mathrm{T}}\Gamma_{F_{i,l}}^{-1}\tilde{\Theta}_{F_{i,l}}\right). \tag{52}$$

Taking time derivative of V_i and substituting Eqs. (29), (40), (44) and (48) into it, we have

$$\begin{aligned}\dot{V}_i = &-\sum_{k=1}^{4}\bar{Z}_{i,k}^{\mathrm{T}}K_{i,k}\bar{Z}_{i,k}+\left(\bar{Z}_{i,2}^{\mathrm{T}}A_{i,1}+\bar{Z}_{i,3}^{\mathrm{T}}A_{i,2}\right)E_{F_{i,1}}\\&+\tilde{\Theta}_{F_{i,1}}^{\mathrm{T}}\left[\Phi_{F_{i,1}}\left(A_{i,1}^{\mathrm{T}}\bar{Z}_{i,2}+A_{i,2}^{\mathrm{T}}\bar{Z}_{i,3}\right)-\Gamma_{F_{i,1}}^{-1}\dot{\hat{\Theta}}_{F_{i,1}}\right]\\&+\tilde{\Theta}_{F_{i,2}}^{\mathrm{T}}\left(\Phi_{F_{i,2}}A_{i,3}^{\mathrm{T}}\bar{Z}_{i,4}-\Gamma_{F_{i,2}}^{-1}\dot{\hat{\Theta}}_{F_{i,2}}\right)\\&+\bar{Z}_{i,4}^{\mathrm{T}}A_{i,3}E_{F_{i,2}}\\&+\bar{Z}_{i,4}^{\mathrm{T}}\sum_{j=1}^{3}E_{B_{i,2j}}u_{i,j}-0.5\left(\left\|\bar{Z}_{i,2}\right\|^2\right.\\&\left.+\left\|\bar{Z}_{i,3}\right\|^2\right)-2\left\|\bar{Z}_{i,4}\right\|^2\\&+\sum_{j=1}^{3}\tilde{\Theta}_{B_{i,2j}}^{\mathrm{T}}\left(\Phi_{B_{i,2j}}\bar{Z}_{i,4}u_{i,j}-\Gamma_{B_{i,2j}}^{-1}\dot{\hat{\Theta}}_{B_{i,2j}}\right).\end{aligned}\tag{53}$$

Then, substituting the adaptive tuning laws (49)–(51) into Eq. (53) gives

$$\begin{aligned}\dot{V}_i = &-\sum_{k=1}^{4}\bar{Z}_{i,k}^{\mathrm{T}}K_{i,k}\bar{Z}_{i,k}+\left(\bar{Z}_{i,2}^{\mathrm{T}}A_{i,1}\right.\\&\left.+\bar{Z}_{i,3}^{\mathrm{T}}A_{i,2}\right)E_{F_{i,1}}+\bar{Z}_{i,4}^{\mathrm{T}}\sum_{j=1}^{3}E_{B_{i,2j}}u_{i,j}\\&-0.5\left(\left\|\bar{Z}_{i,2}\right\|^2+\left\|\bar{Z}_{i,3}\right\|^2\right)-2\left\|\bar{Z}_{i,4}\right\|^2\\&+\bar{Z}_{i,4}^{\mathrm{T}}A_{i,3}E_{F_{i,2}}+\mu_{F_{i,1}}\tilde{\Theta}_{F_{i,1}}^{\mathrm{T}}\hat{\Theta}_{F_{i,1}}\\&+\mu_{F_{i,2}}\tilde{\Theta}_{F_{i,2}}^{\mathrm{T}}\hat{\Theta}_{F_{i,2}}\\&+\sum_{j=1}^{3}\mu_{B_{i,2j}}\tilde{\Theta}_{B_{i,2j}}^{\mathrm{T}}\hat{\Theta}_{B_{i,2j}}.\end{aligned}\tag{54}$$

According to Young's inequality, the following inequality holds

$$\begin{aligned}&\left(\bar{Z}_{i,2}^{\mathrm{T}}A_{i,1}+\bar{Z}_{i,3}^{\mathrm{T}}A_{i,2}\right)E_{F_{i,1}}\\&\leqslant 0.5\left(\left\|\bar{Z}_{i,2}\right\|^2+\left\|\bar{Z}_{i,3}\right\|^2\right.\\&\quad\left.+\left\|A_{i,1}E_{F_{i,1}}\right\|^2+\left\|A_{i,2}E_{F_{i,1}}\right\|^2\right),\end{aligned}\tag{55}$$

$$\begin{aligned}&\bar{Z}_{i,4}^{\mathrm{T}}\left(\sum_{j=1}^{3}E_{B_{i,2j}}u_{i,j}+A_{i,3}E_{F_{i,2}}\right)\\&\leqslant 2\left\|\bar{Z}_{i,4}\right\|^2+1.5\sum_{j=1}^{3}\left\|E_{B_{i,2j}}u_{i,j}\right\|^2\\&\quad+0.5\left\|A_{i,3}E_{F_{i,2}}\right\|^2.\end{aligned}\tag{56}$$

With Cauchy–Schwarz inequality, we have

$$\begin{aligned}\mu_{F_{i,1}}\tilde{\Theta}_{F_{i,1}}^{\mathrm{T}}\hat{\Theta}_{F_{i,1}}&\leqslant\mu_{F_{i,1}}\left(\|\tilde{\Theta}_{F_{i,1}}\|\|\Theta_{F_{i,1}}^*\|-\|\tilde{\Theta}_{F_{i,1}}\|^2\right)\\&\leqslant\frac{\mu_{F_{i,1}}}{2}\left(\|\Theta_{F_{i,1}}^*\|^2-\|\tilde{\Theta}_{F_{i,1}}\|^2\right),\end{aligned}\tag{57}$$

$$\mu_{F_{i,2}}\tilde{\Theta}_{F_{i,2}}^{\mathrm{T}}\hat{\Theta}_{F_{i,2}}\leqslant\frac{\mu_{F_{i,2}}}{2}\left(\|\Theta_{F_{i,2}}^*\|^2-\|\tilde{\Theta}_{F_{i,2}}\|^2\right),\tag{58}$$

$$\mu_{B_{i,2j}}\tilde{\Theta}_{B_{i,2j}}^{\mathrm{T}}\hat{\Theta}_{B_{i,2j}}\leqslant\frac{\mu_{B_{i,2j}}\left(\|\Theta_{B_{i,2j}}^*\|^2-\|\tilde{\Theta}_{B_{i,2j}}\|^2\right)}{2}.\tag{59}$$

Then, substituting Eqs. (55)–(59) into Eq. (54), it follows that

$$\begin{aligned}\dot{V}_i\leqslant&-\sum_{l=1}^{4}\bar{Z}_{i,l}^{\mathrm{T}}K_{i,l}\bar{Z}_{i,l}-\frac{\mu_{F_{i,1}}}{2}\|\tilde{\Theta}_{F_{i,1}}\|^2\\&-\frac{\mu_{F_{i,2}}}{2}\|\tilde{\Theta}_{F_{i,2}}\|^2-\frac{1}{2}\sum_{j=1}^{3}\mu_{B_{i,2j}}\|\tilde{\Theta}_{B_{i,2j}}\|^2+Q_i\end{aligned}\tag{60}$$

where $Q_i = 0.5(\mu_{F_{i,1}}\rho_{F_{i,1}}+\mu_{F_{i,2}}\rho_{F_{i,2}}+\sum_{j=1}^{3}\mu_{B_{i,2j}}\rho_{B_{i,2j}}+\rho_i)$, $\rho_{F_{i,1}} = \max\{\|\Theta_{F_{i,1}}^*\|^2\}$, $\rho_{F_{i,2}} = \max\{\|\Theta_{F_{i,2}}^*\|^2\}$, $\rho_{B_{i,2j}} = \max\{\|\Theta_{B_{i,2j}}^*\|^2\}$, $\rho_i = \max\{\left\|A_{i,1}E_{F_{i,1}}\right\|^2+\left\|A_{i,2}E_{F_{i,1}}\right\|^2+\left\|A_{i,3}E_{F_{i,2}}\right\|^2+\sum_{j=1}^{3}\left\|E_{B_{i,2j}}u_{i,j}\right\|^2\}$

Assumption 1 implies that the optimal weight vectors $\Theta_{F_{i,1}}^*$, $\Theta_{F_{i,2}}^*$ and $\Theta_{B_{i,2j}}^*$ are bounded, so $\rho_{F_{i,1}}$, $\rho_{F_{i,2}}$ and $\rho_{B_{i,2j}}$ exist. ρ_i exists since the side-slip angle β_i is guaranteed to be small near 0, U_i is bounded, and the reconstruction errors $E_{F_{i,1}}$, $E_{F_{i,2}}$ and $E_{B_{i,2j}}$ are bounded.

Define

$$\begin{aligned}&k_{i,l}^* = 2\lambda_{\min}\{K_{i,l}\},\ \gamma_{F_{i,1}}^* = \lambda_{\max}\left\{\Gamma_{F_{i,1}}^{-1}\right\},\\&\gamma_{F_{i,2}}^* = \lambda_{\max}\left\{\Gamma_{F_{i,2}}^{-1}\right\},\ \gamma_{B_{i,2j}}^* = \lambda_{\max}\left\{\Gamma_{B_{i,2j}}^{-1}\right\},\\&\eta_i = \min\left\{k_{i,l}^*,\mu_{F_{i,1}}/\gamma_{F_{i,1}}^*,\mu_{F_{i,1}}/\gamma_{F_{i,1}}^*,\mu_{B_{i,2j}}/\gamma_{B_{i,2j}}^*\right\}\end{aligned}\tag{61}$$

where $i = 1,\ldots,N$, $j = 1,2,3$, $l = 1,\ldots,4$, $\lambda_{\min}\{\cdot\}$ and $\lambda_{\max}\{\cdot\}$ denote the smallest and largest eigenvalue of a matrix, respectively. Then, from Eq. (60), we have

$$\dot{V}_i\leqslant-\eta_i V_i+Q_i\tag{62}$$

Since the Lyapunov function V for all the followers can be chosen as $V = \sum_{i=1}^{N} V_i$, it follows from Eq. (62) that

$$\dot{V} \leqslant -\eta V + Q \tag{63}$$

where $\eta = \min\{\eta_i\}$ and $Q = \sum_{i=1}^{N} Q_i$.

According to Eq. (60), $\bar{Z}_{i,l}$ and $\tilde{\Theta}_{\triangle}$ will converge into the domain $\Omega_{\bar{z}_{i,l}} = \left\{\bar{Z}_{i,l} \middle| \|\bar{Z}_{i,l}\| < \sqrt{\frac{2Q_i}{k^*_{i,l}}}\right\}$ $(i = 1, \ldots, N, l = 1, \ldots, 4)$ and $\Omega_{\tilde{\theta}_{\triangle}} = \left\{\tilde{\Theta}_{\triangle} \middle| \|\tilde{\Theta}_{\triangle}\| < \sqrt{\frac{2Q}{\mu_{\triangle}}}\right\}$ $(\triangle = F_{i,1}, F_{i,2}, B_{i,2j}, j = 1, 2, 3)$, respectively. Therefore, $\bar{Z}_{i,l}$ and $\tilde{\Theta}_{\triangle}$ are CSUUB.

The command filter compensators, described by Eqs. (28), (39), (43) and (47), are actually BIBO stable linear filters. Since each input of these filters are bounded, the output of these filters are bounded as well (i.e., the signals $\xi_{i,l}, i = 1, \ldots, N, l = 1, \ldots, 4$, are bounded). Therefore, the actual tracking errors $Z_{i,l}$ are also CSUUB.

From Eq. (63), we can derive that

$$\begin{aligned} 0 \leqslant V(t) &\leqslant \frac{Q}{\eta} + \left[V(0) - \frac{Q}{\eta}\right] e^{-\eta t} \\ &< \frac{Q}{\eta} + V(0) e^{-\eta t}. \end{aligned} \tag{64}$$

Combined with Eq. (52), the following inequality is satisfied

$$\frac{1}{2}\|\bar{Z}_1\|^2 < V(t) < \frac{Q}{\eta} + V(0) e^{-\eta t}. \tag{65}$$

where $\bar{Z}_1 = [\bar{Z}_{1,1}^{\mathrm{T}}, \ldots, \bar{Z}_{N,1}^{\mathrm{T}}]^{\mathrm{T}}$. This implies that for $\sigma > \sqrt{(2Q/\eta)}$ there exists T such that for all $t \geq T$, $\bar{Z}_1$ satisfies $\|\bar{Z}_1\| < \sigma$. The convergence domain factor σ depends on the controller parameters $(K_{i,l}, \Gamma_{\triangle}, \mu_{\triangle}, \triangle = F_{i,1}, F_{i,2}, B_{i,2j})$ and the BSNN reconstruction errors $E_{\triangle}, \triangle = F_{i,1}, F_{i,2}, B_{i,2j}$. Therefore, to achieve better formation control performance, we can increase $\lambda_{\min}\{K_{i,l}\}$ and $\lambda_{\min}\{\Gamma_{\triangle}\}$, and apply BSNN with more nodes.

The formation tracking error of all the followers, defined in Eq. (17), satisfies

$$\begin{aligned} \|e_f\| = \|A_{LB}^{-1} Z_1\| &\leqslant \|A_{LB}^{-1}\| \|Z_1\| \\ &\leqslant \sqrt{\lambda_{\max}\left\{(A_{LB}^{-1})^{\mathrm{T}} A_{LB}^{-1}\right\}} (\|\bar{Z}_1\| + \|\xi_1\|) \end{aligned} \tag{66}$$

where $A_{LB} = (\mathcal{L} + \mathcal{B}) \otimes I_3$ and $\xi_1 = [\xi_{1,1}^{\mathrm{T}}, \ldots, \xi_{N,1}^{\mathrm{T}}]^{\mathrm{T}}$. If the limit functions of the command filters are not in effect, $\|\xi_1\|$ will converge to zero. Therefore, the formation tracking error of all the followers can be reduced by choosing control parameters properly. □

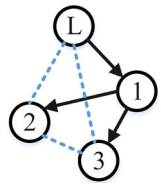

Fig. 2 Communication topology and desired formation structure

5 Numerical simulation

In this section, a numerical simulation under the proposed formation controller is first conducted to illustrate the effectiveness of the proposed algorithm. Then a two-loop formation control method is implement under the same condition for comparison. We will show that the performance of the integrated formation control scheme is better than the two-loop one in large maneuvering flight.

Consider a missile formation with one leader and three followers. As depicted in Fig. 2, the communication topology is a simple directed spanning tree denoted by the solid arrows and the desired formation structure is defined as a regular tetrahedron with each edge being 100 m. Derived from the path planning algorithm and the PN guidance law, the trajectory of the leader is

$$\begin{aligned} &\dddot{r}_x(t) = 0, \quad \dddot{r}_y(t) = 0 \\ &\dddot{r}_z(t) = \begin{cases} 10 & 0\,\mathrm{s} < t \leqslant 2\,\mathrm{s}, 14\,\mathrm{s} < t \leqslant 16\,\mathrm{s} \\ -10 & 6\,\mathrm{s} < t \leqslant 10\,\mathrm{s} \\ 0 & \text{otherwise.} \end{cases} \end{aligned} \tag{67}$$

where the initial values are $r(0) = (0, 100, 3081.65)^{\mathrm{T}}$, $\dot{r}(0) = (250, 50, 0)^{\mathrm{T}}$ and $\ddot{r}(0) = (0, 0, 0)^{\mathrm{T}}$.

Each follower has the same nominal parameters which are listed in Table 1. The average air density ρ_i is calculated by $\rho_i = 1.225(1 - \frac{h_i}{44300})^{4.2533}$, where h_i is the flight altitude of the ith follower. The initial positions of three followers are $X_{1,1} = (10, 90, 3000)^{\mathrm{T}}$, $X_{2,1} = (-38.9, 60, 3010)^{\mathrm{T}}$ and $X_{3,1} = (-38.9, 80, 2960)^{\mathrm{T}}$. The initial velocity, flight path angle and heading angle of each follower are, respectively, set as $V_i(0) = 254$ m/s, $\theta_i(0) = 11.3°$ and $\psi_{V_i}(0) = 0°$. The initial angle of attack, sideslip angle and bank angle are, respectively, set as $\alpha_i(0) = 3°$, $\beta_i(0) = \gamma_{V_i}(0) = 0°$. The initial angu-

Table 1 Nominal parameters of follower i

Parameter	Value	Parameter	Value
m_i	400 kg	g	9.8 kg/m^2
l_i	0.5 m	b_{Ai}	0.4 m
S_i	0.52 m^2	J_{xi}	100 kg m^2
J_{yi}	1300 kg m^2	J_{zi}	1200 kg m^2

Table 2 Initial values of the estimated coefficients

Coefficient	Value	Coefficient	Value
$\hat{C}_{D_i0}(0)$	0.05	$\hat{C}^{\alpha}_{D_i}(0)$	4.9
$\hat{C}^{\beta}_{Y_i}(0)$	− 1.9	$\hat{C}_{L_i0}(0)$	0.1
$\hat{C}^{\alpha}_{L_i}(0)$	2.4	$\hat{m}^{\beta_i}_{xi}(0)$	− 0.3
$\hat{m}^{\omega_{xi}}_{xi}(0)$	− 0.29	$\hat{m}^{\delta_{xi}}_{xi}(0)$	16
$\hat{m}^{\beta_i}_{yi}(0)$	− 14.5	$\hat{m}^{\omega_{yi}}_{yi}(0)$	− 2.9
$\hat{m}^{\delta_{yi}}_{yi}(0)$	− 17	$\hat{m}^{\alpha_i}_{zi}(0)$	− 18.7
$\hat{m}^{\omega_{zi}}_{zi}(0)$	− 2.9	$\hat{m}^{\delta_{zi}}_{zi}(0)$	− 24

lar rates and control surface deflections are all set as zero.

The third-order B-Spline functions are used as the basis functions of BSNN for each follower. In order to construct the basis functions, we set that the range of the angle of attack α_i is $[-8°, 12°]$ with 11 knots spaced every 2°; the range of the side-slip angle β_i is $[-5°, 5°]$ with 6 knots spaced every 2°; the speed V_i, expressed in Mach numbers, is in the range of [0.5, 0.9] with 5 knots spaced every 0.1 Ma. The third-order spline basis functions with n nodes consist of $(n+1)$ pieces. The coefficient $C_{D_i0}(V_i)$ is approximated by BSNN with univariate B-spline basis functions owning 6 nodes in the hidden layer. The coefficient $C^{\alpha_i}_{D_i}(\alpha_i, V_i)$ is approximated by BSNN with bivariate B-spline basis functions whose hidden layer is of 72 nodes. Other coefficients are approximated similarly. The aerodynamic data we use in this simulation come from [29]. The initial values of the estimated aerodynamic coefficients are displayed in Table 2. Each aerodynamic coefficient has $+10\%$ uncertainty in the form of $C_*(t)\sin(\frac{t}{5})$, where $C_*(t)$ is a generic marker to represent any of the aerodynamic coefficients.

The ω_n in four command filters are selected as $(15, 10, 10)^{\mathrm{T}}$, $(25, 20, 20)^{\mathrm{T}}$, $(35, 35, 35)^{\mathrm{T}}$ and $(40, 40, 40)^{\mathrm{T}}$. The damping factor in each filter is 0.707. The constraints on the states and control surfaces adopted in the command filters are listed in Table 3.

Table 3 Constraints on states and control surfaces

Variable	Magnitude limit
α_i	$[-8, 12]$ deg
β_i	$[-5, 5]$ deg
γ_{V_i}	$[-90, 90]$ deg
ω_{xi}	$[-130, 130]$ deg/s
ω_{yi}, ω_{zi}	$[-30, 30]$ deg/s
$\delta_{xi}, \delta_{yi}, \delta_{zi}$	$[-15, 15]$ deg

The control parameters for three followers are chosen as $K_{1,1} = \mathrm{diag}(1, 1.3, 1.2)$, $K_{2,1} = \mathrm{diag}(1.3, 1.6, 1)$, $K_{3,1} = \mathrm{diag}(1.2, 1.5, 1.2)$, $K_{1,2} = \mathrm{diag}(1.9, 0.7, 0.6)$, $K_{2,2} = \mathrm{diag}(2, 0.9, 0.4)$, $K_{3,2} = \mathrm{diag}(2.2, 0.8, 0.6)$, $K_{1,3} = K_{2,3} = K_{3,3} = \mathrm{diag}(3, 3, 3)$, and $K_{1,4} = K_{2,4} = K_{3,4} = \mathrm{diag}(5, 5, 5)$. Set $\mu_{F_{i,1}} = 0.03$, $\mu_{F_{i,2}} = \mu_{B_{i,21}} = \mu_{B_{i,22}} = 0.01$, and $\mu_{B_{i,23}} = 0.001$, for $i = 1, 2, 3$. And choose $\Gamma_{F_{i,1}} = \mathrm{diag}\{100 \cdot \mathbf{1}^{\mathrm{T}}_{78}, 900 \cdot \mathbf{1}^{\mathrm{T}}_{72}, 100 \cdot \mathbf{1}^{\mathrm{T}}_{6}, 700 \cdot \mathbf{1}^{\mathrm{T}}_{72}\}$, $\Gamma_{F_{i,2}} = \mathrm{diag}\{100 \cdot \mathbf{1}^{\mathrm{T}}_{7}, 40 \cdot \mathbf{1}^{\mathrm{T}}_{6}, 80 \cdot \mathbf{1}^{\mathrm{T}}_{31}\}$, and $\Gamma_{B_{i,21}} = \Gamma_{B_{i,22}} = \Gamma_{B_{i,23}} = 50 I_{18}$ $(i = 1, 2, 3)$.

Under the proposed formation control law with the above parameters, the trajectories of each missile in the formation are plotted in Fig. 3. The leader flies at the high trajectory, while the three followers fly at lower trajectories in the same plane. Figure 4 illustrates that the followers can form and maintain the desired formation structure. As depicted in Figs. 5 and 6, the position and velocity tracking errors of each follower converge to zero which reveals that the three followers are capable of following the trajectory of the leader precisely. So we can conclude that the followers are able to follow the leader while maintaining a predetermined formation under the control of the proposed distributed controller.

Benefiting from the use of command filters, the attitude angles and angular rates of three followers, shown in Figs. 7 and 8, satisfy their own constraints which are listed in Table 3. Meanwhile, it is worth noting that the side-slip angles β_i (depicted in Fig. 7b) are successfully stabilized near 0°, so that the coordinated turn is able to be achieved. The control surface deflections δ_{xi}, δ_{yi} and δ_{zi}, plotted in Fig. 9, are not more than 15° in both directions, which indicates that the physical limitations of servo motors are satisfied.

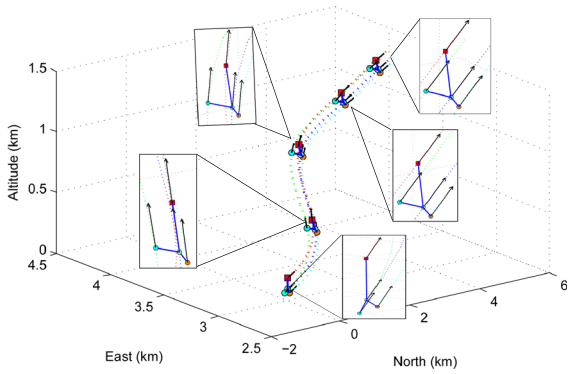

Fig. 3 Trajectory of the formation flying

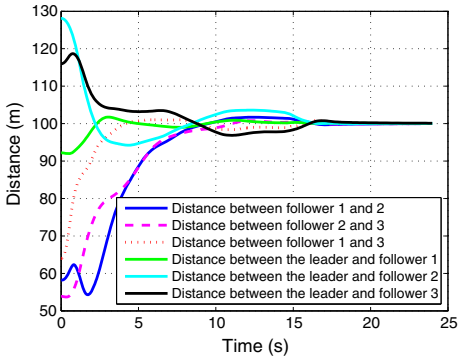

Fig. 4 Distance between each two missiles in the formation

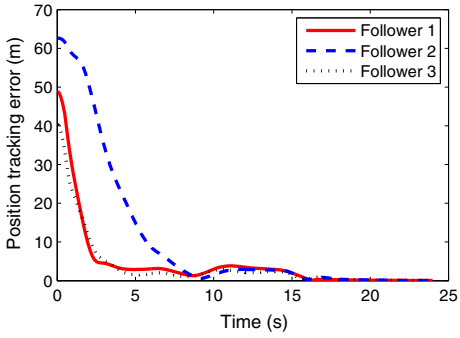

Fig. 5 Position tracking errors of three followers

Then another simulation is conducted using the constraint force (CF) formation control method in [12] under the same initial conditions mentioned before. The CF method adopts a two-loop formation control scheme, and its simulation results are presented in Figs. 10, 11 and 12. Compared with Figs. 4, 5 and 6, we notice that the plots of the position and velocity tracking errors in Figs. 11 and 12 have larger overshoots over the period from 10 to 16 s, when the formation is desired to

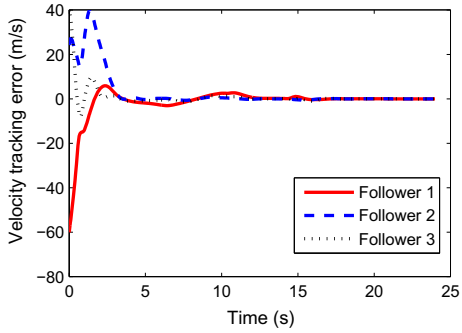

Fig. 6 Velocity tracking errors of three followers

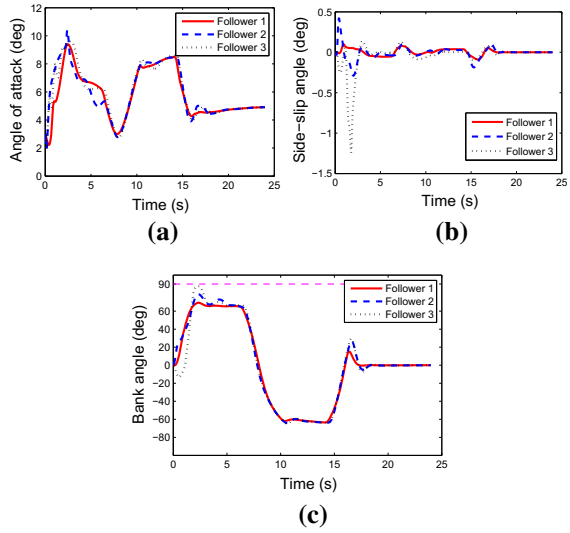

Fig. 7 Attitude angles of followers. **a** Angle of attack, **b** side-slip angle, **c** bank angle

make a turn. This is because the inner-loop controllers are not able to track the attitude angle commands generated from the outer-loop controllers quickly in the CF method when making a turn. It implies that the two control loops are not coordinated, which degrades the formation tracking performance during the large maneuvering bank-to-turn. However, our proposed method is capable of making the two control loops work synergistically and achieving a coordinated turn, which ensures good maneuverability for the whole formation flight.

6 Conclusion

The missile formation control problem with leader-following formation structure in 3-D space is investigated in this paper. An integrated backstepping-based

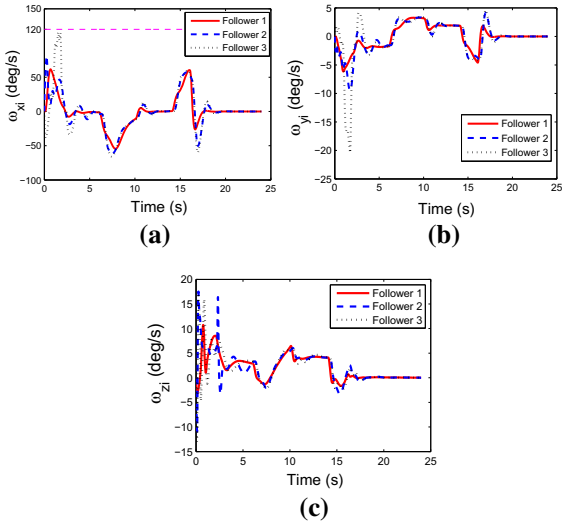

Fig. 8 Angular rates of followers. **a** Roll rates, **b** yaw rates, **c** pitch rates

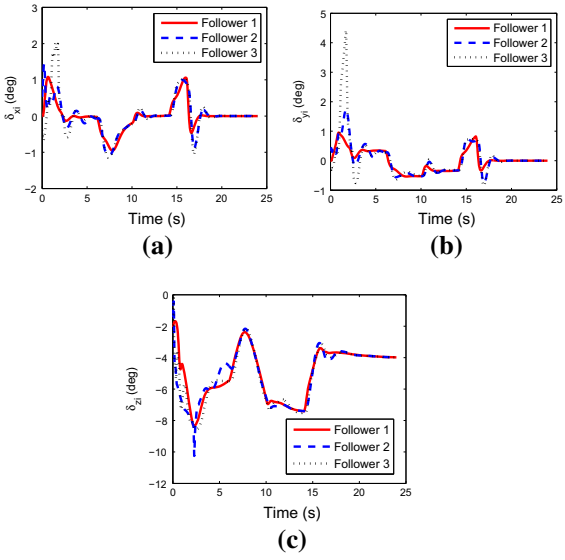

Fig. 9 Control surface deflections of followers. **a** δ_{xi}, **b** δ_{yi}, **c** δ_{zi}

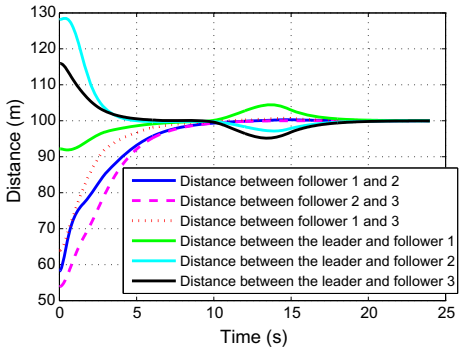

Fig. 10 Distance between each two missiles in the formation using CF method

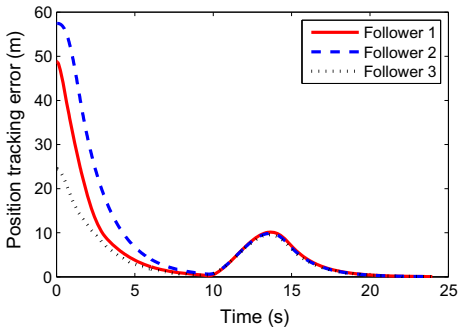

Fig. 11 Position tracking errors using CF method

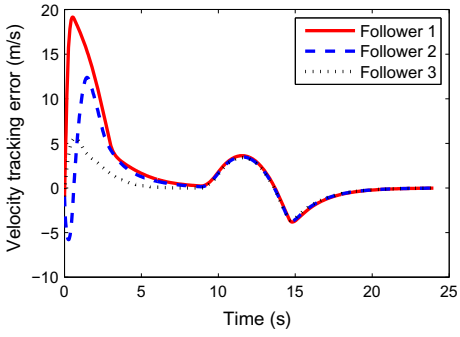

Fig. 12 Velocity tracking errors using CF method

control scheme is proposed to handle both formation control and attitude control in large maneuvering flight. With the help of the command filters and BSNN, the proposed formation control algorithm can also deal with the state constraints, actuator saturations and uncertain aerodynamic coefficients. The distributed formation control law guarantees that all the states in the closed-loop systems are CSUUB, and the formation tracking errors are small enough by appropriately tuning the control parameters. Two numerical simulations illustrate the effectiveness of the proposed formation control algorithm and the good performance in the large maneuvering formation flight. Future work may further investigate the problem of formation transformation and obstacle avoidance in the formation flight.

Acknowledgements This work was supported by Projects of Major International (Regional) Joint Research Program

NSFC (Grant No. 61720106011), NSFC (Grant Nos. 61573062, 61621063, 61673058 and 61603094), Beijing Education Committee Cooperation Building Foundation Project (Grant No. 2017CX02005), Beijing Advanced Innovation Center for Intelligent Robots and Systems (Beijing Institute of Technology), Key Laboratory of Biomimetic Robots and Systems (Beijing Institute of Technology), Ministry of Education, Beijing, 100081, China.

References

1. Shiyu, Z., Rui, Z.: Cooperative guidance for multimissile salvo attack. Chin. J. Aeronaut. **21**(6), 533–539 (2008)
2. Shaferman, V., Shima, T.: Cooperative optimal guidance laws for imposing a relative intercept angle. J. Guid. Control Dyn. **38**(8), 1395–1408 (2015)
3. Song, J., Song, S., Xu, S.: Three-dimensional cooperative guidance law for multiple missiles with finite-time convergence. Aerosp. Sci. Technol. **67**, 193–205 (2017)
4. Zhao, J., Zhou, S., Zhou, R.: Distributed time-constrained guidance using nonlinear model predictive control. Nonlinear Dyn. **84**(3), 1399–1416 (2016)
5. Zhao, J., Zhou, R.: Unified approach to cooperative guidance laws against stationary and maneuvering targets. Nonlinear Dyn. **81**(4), 1635–1647 (2015)
6. Cui, N., Wei, C., Guo, J., Zhao, B.: Research on missile formation control system. In: Proceedings of the 2009 IEEE International Conference on Mechatronics and Automation, pp. 4197–4202. Changchun, China, August 9–12 (2009)
7. Wei, C., Shen, Y., Ma, X., Guo, J., Cui, N.: Optimal formation keeping control in missile cooperative engagement. Aircr. Eng. Aerosp. Technol. **84**(6), 376–389 (2012)
8. Wei, C., Guo, J., Lu, B., Shen, Y., Zhang, L.: Adaptive control for missile formation keeping under leader information unavailability. In: 10th IEEE International Conference on Control and Automation (ICCA), pp. 902–907. Hangzhou, China, June 12–14 (2013)
9. Wang, Y., Wang, Y., Sun, M., Du, S., Chen, Z.: Neural networks based formation control of anti-ship missiles with constant velocity. In: 2015 IEEE International Conference on Computer and Information Technology; Ubiquitous Computing and Communications; Dependable, Autonomic and Secure Computing; Pervasive Intelligence and Computing (CIT/IUCC/DASC/PICOM), pp. 2151–2156. Liverpool, UK, October 26–28 (2015)
10. Qiu, H., Duan, H.: Receding horizon control for multiple UAV formation flight based on modified brain storm optimization. Nonlinear Dyn. **78**(3), 1973–1988 (2014)
11. Chen, Q., Wan, J., Ai, J.: L_1 adaptive controller design for hypersonic formation flight. Sci. China Technol. Sci. **59**(10), 1597–1608 (2016)
12. Zou, Y., Pagilla, P.R., Ratliff, R.T.: Distributed formation flight control using constraint forces. J. Guid. Control Dyn. **32**(1), 112–120 (2009)
13. Van Soest, W.R., Chu, Q.P., Mulder, J.A.: Combined feedback linearization and constrained model predictive control for entry flight. J. Guid. Control Dyn. **29**(2), 427–434 (2006)
14. Su, H., Chen, M.Z., Lam, J., Lin, Z.: Semi-global leader-following consensus of linear multi-agent systems with input saturation via low gain feedback. IEEE Trans. Circuits Syst. I Regul. Pap. **60**(7), 1881–1889 (2013)
15. Wang, H., Wang, D., Peng, Z.: Adaptive dynamic surface control for cooperative path following of marine surface vehicles with input saturation. Nonlinear Dyn. **77**(1–2), 107–117 (2014)
16. Yang, T., Meng, Z., Dimarogonas, D.V., Johansson, K.H.: Global consensus for discrete-time multi-agent systems with input saturation constraints. Automatica **50**(2), 499–506 (2014)
17. Massari, M., Bernelli-Zazzera, F., Canavesi, S.: Nonlinear control of formation flying with state constraints. J. Guid. Control Dyn. **35**(6), 1919–1925 (2012)
18. Alamir, M., Murilo, A.: Swing-up and stabilization of a Twin-Pendulum under state and control constraints by a fast NMPC scheme. Automatica **44**(5), 1319–1324 (2008)
19. Dong, W., Farrell, J.A., Polycarpou, M.M., Djapic, V., Sharma, M.: Command filtered adaptive backstepping. IEEE Trans. Control Syst. Technol. **20**(3), 566–580 (2012)
20. Farrell, J., Polycarpou, M., Sharma, M.: On-line approximation based control of uncertain nonlinear systems with magnitude, rate and bandwidth constraints on the states and actuators. In: Proceedings of the 2004 American Control Conference, vol. 3, pp. 2557–2562. Boston, MA, USA, June 30–July 2 (2004)
21. Farrell, J.A., Polycarpou, M., Sharma, M., Dong, W.: Command filtered backstepping. IEEE Trans. Autom. Control **54**(6), 1391–1395 (2009)
22. Ren, W., Beard, R.W.: Distributed Consensus in Multi-vehicle Cooperative Control, p. 31. Springer, London (2008)
23. Qian, X., Lin, R., Zhao, Y.: Missile Flight Dynamics, pp. 29–36. Beijing Institute of Technology Press, Beijing (2000)
24. Sonneveldt, L., Chu, Q.P., Mulder, J.A.: Nonlinear flight control design using constrained adaptive backstepping. J. Guid. Control Dyn. **30**(2), 322–336 (2007)
25. Sharma, M., Farrell, J., Polycarpou, M., Richards, N., Ward, D.: Backstepping flight control using on-line function approximation. In: AIAA Guidance, Navigation, and Control Conference and Exhibit, Austin, Texas, August 11–14 (2003)
26. Farrell, J.A., Polycarpou, M.M.: Adaptive Approximation Based Control: Unifying Neural, Fuzzy and Traditional Adaptive Approximation Approaches, pp. 80–84. Wiley, Hoboken (2006)
27. Farrell, J., Sharma, M., Polycarpou, M.: Backstepping-based flight control with adaptive function approximation. J. Guid. Control Dyn. **28**(6), 1089–1102 (2005)
28. Brent, R.P.: Algorithms for Minimization Without Derivatives, pp. 61–79. Dover Publications, Mineola (2013)
29. Du, H.: Adaptive block dynamic surface control for BTT missile attitude control system. Dissertation for the Master Degree, Harbin Institute of Technology, China (2012)